ResearchGate

See discussions, stats, and author profiles for this publication at: https://www.researchgate.net/publication/231644495

Electronic Structures and Optical Properties of 6H- and 3C-SiC Microstructures and Nanostructures from X-ray Absorption Fine Structures, X-ray Excited Optical Luminescence, and The...

ARTICLE *in* THE JOURNAL OF PHYSICAL CHEMISTRY C · MARCH 2010

Impact Factor: 4.77 · DOI: 10.1021/jp100277s

CITATIONS
11

READS
41

3 AUTHORS, INCLUDING:

Lijia Liu
Soochow University (PRC)
31 PUBLICATIONS **290** CITATIONS
SEE PROFILE

Yun-Mui Yiu
The University of Western Ontario
40 PUBLICATIONS **370** CITATIONS
SEE PROFILE

Available from: Yun-Mui Yiu
Retrieved on: 23 January 2016

Electronic Structures and Optical Properties of 6H- and 3C-SiC Microstructures and Nanostructures from X-ray Absorption Fine Structures, X-ray Excited Optical Luminescence, and Theoretical Studies

Lijia Liu, Y. M. Yiu, and T. K. Sham*

Department of Chemistry, University of Western Ontario, London, Ontario, Canada N6A 5B7

Liying Zhang and Yafei Zhang*

National Key Laboratory of Nano/Micro Fabrication Technology, Key Laboratory for Thin Film and Microfabrication of the Ministry of Education, Research Institute of Micro/Nano Science and Technology, Shanghai Jiao Tong University, Shanghai 200240, P. R. China

Received: January 11, 2010; Revised Manuscript Received: March 13, 2010

We report a comparative study of the electronic and optical properties of five silicon carbide (SiC) materials of different crystal structures (6H and 3C polytypes), sizes (micro- and nanocrystals), and morphologies (nanowires of SiC−SiO_2 core−shell structures and oxide-free nanowires). X-ray absorption near-edge structures (XANES) at both Si K- and C K-edge have been used to investigate the electronic structures of SiC. Theoretical calculations using density functional theory (DFT), the WIEN2k code are in good accord with the experiment. It is found that both 6H- and 3C-SiC have similar XANES at Si K-edge hence similar local structure at the Si site but slightly and more noticeable difference at the C K-edge, which is due to the difference in band gaps among the polytypes. The spectra of core−shell nanowires are found to have both SiO_2 and SiC contributions in which SiO_2 is dominant. The SiO_2 shell can be almost completely removed by hydrofluoric acid treatment. X-ray excited optical luminescence (XEOL) was used to measure light emission from SiC by tuning the excitation photon energy across both Si K- and C K-edge. Luminescence was observed from all SiC samples upon X-ray excitation, though at different wavelengths depending on the crystal structures and morphologies. By measuring the yield of the total luminescence (300−800 nm) and luminescence at selected wavelengths with excitation photon energy across the absorption edge, we are able to ascribe the luminescence at various wavelengths to surface states and defects, quantum confinement, and SiO_2 surface/SiC-SiO_2 interface in core−shell nanowires. The implications of these findings are discussed.

Introduction

Silicon carbide (SiC) has a variety of unique properties. It is of highly chemical inertness and good thermal conductivity and thus regarded as a promising substitute for silicon in fabricating devices which operate in extreme conditions (i.e., high temperature and high power).[1,2] The SiC crystal structure has many modifications, referred to as polytypes, but all of them consist of close-packed Si−C tetrahedral units, in which Si and C atoms are linked through a sp^3 bonding network. The commonly found SiC polytypes are denoted 6H-, 4H-, 2H-, and 3C-SiC, which differ in the stacking sequence of Si−C tetrahedral units. The character in the labeling represents the types of crystal systems (i.e., H for hexagonal and C for cubic) and the number refers to the layers of Si−C per unit cell. All SiC polytypes are indirect band gap semiconductors. The band gap of SiC increases with increasing hexagonal character in the polytypes, e.g., 2.39 eV in 3C-SiC, 3.02 eV in 6H-SiC, and 3.33 eV in 2H-SiC.[3] So far, most studies on SiC were done on 6H-SiC and 3C-SiC, which are the most stable and the easiest to obtain; thus, they are promising for industrial applications. 6H-SiC single crystal can be grown in high quality in industry at high temperature (i.e., >1700 °C), while 3C-SiC requires lower temperature but can only be grown under a more controlled condition. The advantages of 6H-SiC are its high breakdown field strength due to the large band gap and commercial availability.[4] Compared to 6H-SiC, 3C-SiC has a smaller band gap but higher electron mobility and oxide coated 3C-SiC nanostructure has been reported to be a good candidate for photocatalysis.[5]

There have been many studies on the electronic structures of SiC polytypes both experimentally and theoretically. Though having the same Si−C tetrahedral local structure, the band structure becomes increasingly complicated as the complexity of the crystal structure increases. Ab initio pseudopotential calculations have been used widely for studying the ground-state electronic structures of SiC polytypes,[6−9] and the results show that the valence band structure of SiC is very similar regardless of the polytype. However, the unoccupied density of states (DOS)/conduction band shows noticeable differences among various SiC polytypes; thus, it has been considered that the differences in the unoccupied DOS play a major role in causing a variation in the energy of the band gap.[8] Despite many theoretical calculations on SiC polytypes, experimental results are relatively lacking. In addition, luminescence from SiC materials has been widely studied as the wide band gap of SiC makes it a good light-emitting material.[10] It is known that bulk SiC exhibits weak photoluminescence (PL) at 600 nm at low temperature, which is assigned to donor−acceptor recombination.[11,12] SiC of micro- and nanostructures, on the other hand,

* Corresponding authors. (T.K.S.) Tel: 1-519-611-2111ext. 8634. Fax: 1-519-3022. E-mail: tsham@uwo.ca. (Y.Z.) Tel: 86-21-34205665. Fax: 86-21-34205665. E-mail: yfzhang@sjtu.edu.cn.

10.1021/jp100277s © 2010 American Chemical Society
Published on Web 03/25/2010

are found to emit light with significantly increased intensity compared to its bulk counterpart. Porous SiC, which is made by electrochemically etching SiC wafer (mostly 6H-SiC), exhibit blue-green PL and the luminescence shows high stability under irradiation and oxidation.[13] This makes SiC an attractive light-emitting material in the fields of micro- and nanoelectronic and optic devices. The origin of luminescence has been widely discussed. Unlike red luminescence from porous Si, which is usually attributed to quantum confinement effect, luminescence from porous SiC in most cases is found below the band gap energy, thus most of the previous studies attributed the PL to surface-related defects.[14−16] Luminescence from other SiC nanostructures, such as SiC nanocrystal embedded matrix,[17,18] SiC nanowires,[19,20] and SiC-SiO_2 complexes,[21] commonly found in 3C-phase, has been reported with luminescence in the range of 400−600 nm. The origin of the luminescence is still not clearly understood. As 3C-SiC has a narrower band gap (2.39 eV, 515 nm), the luminescence can be attributed to band gap emission blue-shifted due to quantum confinement.[22] On the other hand, the luminescence may also come from SiO_2, as SiO_2 has a well-known emission band at ∼460 nm due to oxygen vacancy, and thermally synthesized SiC is usually covered by a thin layer of surface oxide.[17]

In this paper, we present a comparative study on the electronic structure and optical properties of four micro- and nanostructured SiC of 6H- and 3C-phase using X-ray absorption near-edge structures (XANES) and X-ray excited optical luminescence (XEOL). XANES is a spectroscopic technique that monitors the absorption coefficient using tunable X-ray from a synchrotron light source. In XANES, we scan the excitation photon energy from below to about 50 eV above the absorption threshold (edge) of the absorbing atom in a chemical environment and measure the absorption coefficient. It is site and element specific and can provide information on the unoccupied DOS above the Fermi level of the materials of interest. For low z elements such as C and Si, the core levels are in the soft X-ray region and measurements are often conducted in vacuum in total electron yield (TEY) and total X-ray fluorescence yield (FLY), which are relatively surface and bulk sensitive, respectively. These measuring techniques are also ideally suited for the study of thin films.[23] To assist the interpretation of the experimental XANES, theoretical calculation based on density functional theory (DFT) is also conducted for comparative study. These calculations provide band structures and densities of states (DOS) information as well as simulated XANES at the edge of interest.

XEOL is an X-ray photon-in, optical photon-out technique,[24] which monitors the light emission in the UV and visible region excited by the absorption of X-ray and it can be site and excitation channel specific when the incoming photon energy is tuned from below to above an absorption edge of interest. By exciting a core electron to the previously unoccupied state (bottom of the conduction band in the case of SiC), or into the continuum, a core hole is produced, followed by a de-excitation process by which the core hole is filled by shallower core level or valence electrons, leading to X-ray fluorescence and Auger decay (dominant in low z atoms). This cascade process produces electrons and holes which thermalize in the solid resulting in electrons in the bottom of the conduction band and holes at the top of the valence band. Thus the luminescence is produced by either the radiative recombination of a hole in valence band and an electron in conduction band (via the de-excitation path of excitons) leading to the so-called near-band gap emission, or due to defect state in the band gap resulting from vacancies forming electron or hole traps or impurity atoms. XEOL is often recorded with either a conventional optical monochromator by scanning the grating or a dispersive optical element with a CCD detector (spectrograph).

In a recent preliminary study, we conducted XANES and XEOL measurements on 6H-SiC microcrystals and 3C-SiC nanowires.[25] The results show that the XANES of SiC at the near-edge region show very similar features regardless of crystal phases. Also, we found that under X-ray excitation, 6H-SiC microcrystals emit bright light at 600 nm. Meanwhile, bright luminescence from core−shell-structured SiC nanowires of the 3C polytype was also observed but at a different region (∼460 nm).

In this paper, in addition to the 6H-SiC microcrystal and 3C-SiC/SiO_2 core/shell nanowires, two more SiC samples, 6H-SiC and 3C-SiC nanocrystals, are also studied for a systematic comparison. A detailed analysis is conducted on the electronic structure based on Si K-edge and C K-edge XANES results, both experimentally and theoretically. For the optical properties study, XEOL is used in combination with XANES, i.e., that the optical emission is used to track the absorption across the edge. This technique is known as photoluminescence yield (PLY) XANES. PLY XANES can be recorded by counting the total luminescence intensity (zero order) from the entire emission spectrum (typically 200−900 nm) or partial luminescence intensity at selected wavelength windows as the excitation energy is scanned from below to above the absorption edge.[24,26] It is thus used to reveal the structural information of the absorption site which is responsible for the luminescence.

Experimental and Calculation Procedures

Two 6H-SiC microcrystals and three 3C-SiC nanostructured samples have been investigated. The 6H-SiC microcrystals (henceforth denoted 6H-SiCmc, 200−450 mesh particle size) were obtained from Aldrich. Figure 1a shows the scanning electron microscopy (SEM, LEO1530) image of 6H-SiCmc. The SiC crystals are of irregular shapes with the average diameter about 50 μm. The other 6H-SiC microstructure, henceforth denoted 6H-SiCpd is ∼1 μm crystallites and the 3C-SiC nanocrystals (henceforth denoted 3C-SiCpd, 45−55 nm crystallites) were from Alfa Aesar.

The 3C-SiC nanowires were synthesized via a thermal evaporation method in a vertical high-frequency induction furnace, which consists of a quartz tube and an inductive heat cylinder crucible of high-purity graphite. An activated carbon fiber (ACF) layer was packed outside of the graphite crucible.[27] The SiO powder, used as the source material, was placed into the graphite crucible. The system was rapidly heated to 1450 °C within 2 min and maintained for 15 min under high purity Ar. The SiO gas was carried to the active carbon fiber surface by Ar, and the deposition reaction took place on the ACF surface. Then, a light-blue fluffy solid piece layer of SiC nanowires was obtained. Figure 1b shows the SEM image of the as-made SiC nanowires. It can be seen that the nanowires have high purity and are free-standing with diameters of ∼50 nm and a few-micrometer long. The as-made SiC nanowires has a SiC-core-SiO_2-shell structure, as characterized by transmission electron microscopy (TEM, JEM-2010) (see Figure 1c), and is thus denoted SiC/SiO_2-nw. The X-ray diffraction pattern (Figure 1d) shows that the SiC core has a cubic crystal structure (3C-phase). To remove the SiO_2 shell, the as-made nanowires were immersed into a 5% HF solution for 3 min and then rinsed with water. The HF-treated SiC/SiO_2-nw is henceforth denoted SiCnw.

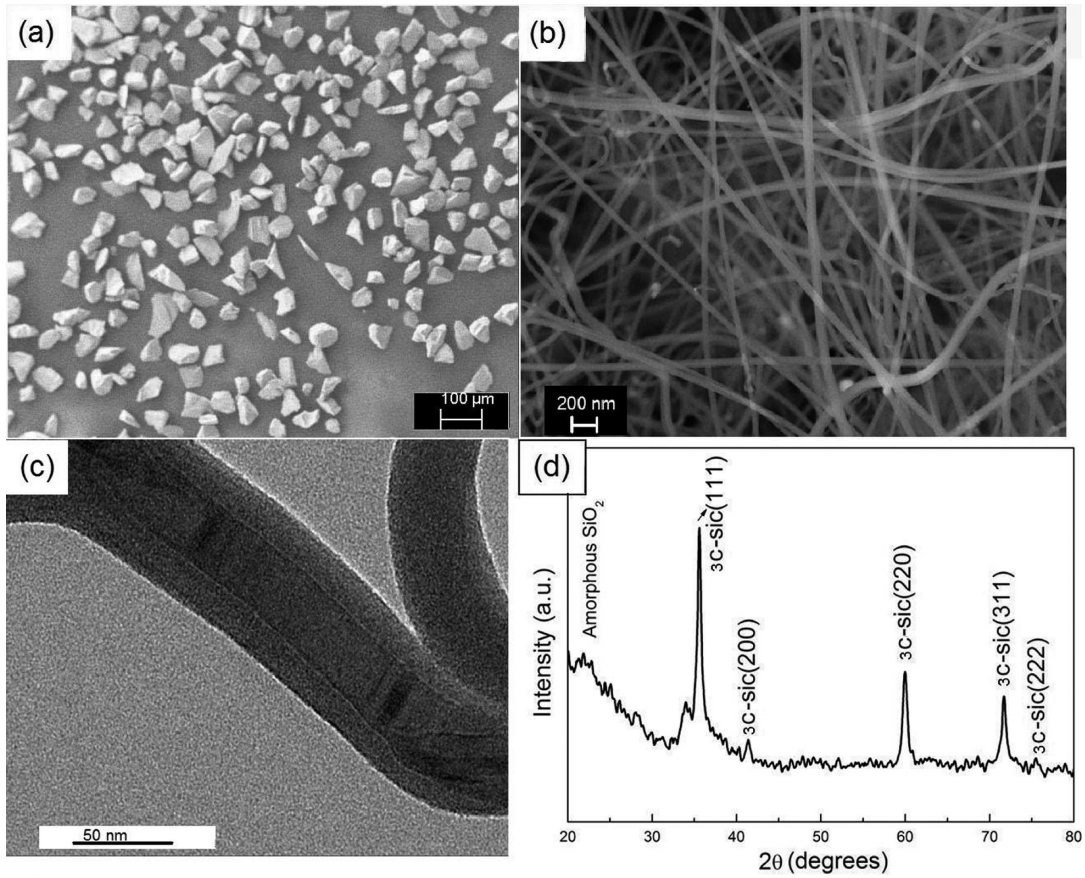

Figure 1. Morphologies of SiC materials: (a) SEM of 6H-SiCmc; (b) SEM of SiC/SiO_2-nw; (c) TEM of SiC/SiO_2-nw; and (d) XRD patterns of SiC/SiO_2-nw.

Synchrotron measurements were performed at the spherical grating monochromator (SGM) beamline at the Canadian Light Source (CLS), the University of Saskatchewan.[28] The samples were mounted on indium foils (the conventional carbon tapes will interfere the spectra during carbon K-edge measurements) and faced at 45° toward the photon beam. XANES were recorded in total electron yield (TEY), X-ray fluorescence yield (FLY), and photoluminescence yield (PLY) where applicable. The TEY was detected with the specimen current and the FLY was measured by detecting the X-ray fluorescence photons using a micro channel plate. XEOL spectra were collected using a dispersive optical spectrometer (QE65000, Ocean Optics). All spectra were normalized to the incident photon flux collected on a refreshed Au grid.

The electronic structures of SiC have been calculated using the density functional theory (DFT)[29,30] together with generalize gradient approximation (GGA).[31] The full potential augmented plane wave method was utilized in the numerical calculation employing the WIEN2k code.[32,33] The crystal structures of 6H-SiC and 3C-SiC are shown in Figure 2,[34] with the crystallographic parameters defined as follows: in the 6H-phase, SiC is hexagonal with the space group of $P6_3mc$, and the lattice constant is $a = 3.073$ Å, $c = 15.08$ Å. The Si and C atoms occupy the 2a (0,0,u) and 2b (1/3,2/3,v) positions with u[Si] = 1/8, v[Si] = 7/24, 23/24, u[C] = 0, and v[C] = 1/6, 5/6. For 3C-SiC, the zincblende crystal structure with the symmetry group of $F\bar{4}3m$ and lattice constant $a = 4.358$ Å are used, in which the Si atom is located at the 4a position of (0,0,0) and the C atom is at the 4c position of (1/4,1/4,1/4).[35,36] The atomic sites are represented by spherical bases sets, which are generated by a linear combination of radial wave functions and nonoverlapping spherical harmonics. The interstitial regions are expressed by a set of 10000 plane waves. The boundary condition between the atomic sites and the interstitial areas satisfies the Dirichlet boundary condition. In this numerical calculation, the tetrahedron method[37] for the **k** space integration was used. The theoretical XANES spectra were then calculated using the electrical dipole transition, convoluted by instrumental Gaussian and core-hole lifetime Lorentzian broadenings.[38] The core-hole lifetime of the K-shell of Si is typically 0.48 eV and that of the K-shell of C is smaller than 0.2 eV.[38]

Results and Discussions

1. Electronic Structures of SiC (Experimental XANES and Theoretical Calculations). ***Si K-Edge XANES.*** Figure 3 shows the Si K-edge XANES of 6H-SiCpd, 6H-SiCmc, and 3C-SiCpd. Let us first take a look at 6H-SiCpd and 6H-SiCmc; both are in the 6H-phase with an approximate crystallite size of 50 and 1 μm, respectively. The TEY of both samples look identical: a shoulder at 1841 eV, three peaks at 1846, 1852, and 1860 eV, which are the characteristic features in SiC.[39] The peak of the highest intensity, the 1846 eV resonance, is attributed to the excitation from Si 1s to Si 3p—C 2sp hybridized states.[40,41] The resonances at higher energies correspond to the unoccupied DOS of p character due to multiple scattering. The FLY shows similar features as TEY but the peaks are broadened and strongly attenuated. This is due to self-absorption (thickness effect),[42−44] as the X-ray one-absorption length at the Si K-edge (~1.26 μm)[45] is smaller than the crystal sizes and the fluorescence X-ray was partially reabsorbed by the sample. There is less attenuation in the FLY of 6H-SiCpd due to a reduced particle size (~1 μm) but still not small enough to alleviate the phenomena. The

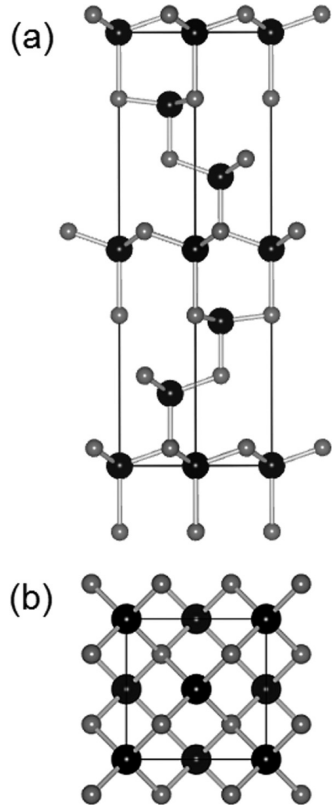

Figure 2. Sketch of SiC crystal structures: (a) 6H-SiC and (b) 3C-SiC. Si atoms in black, and C atoms in gray.

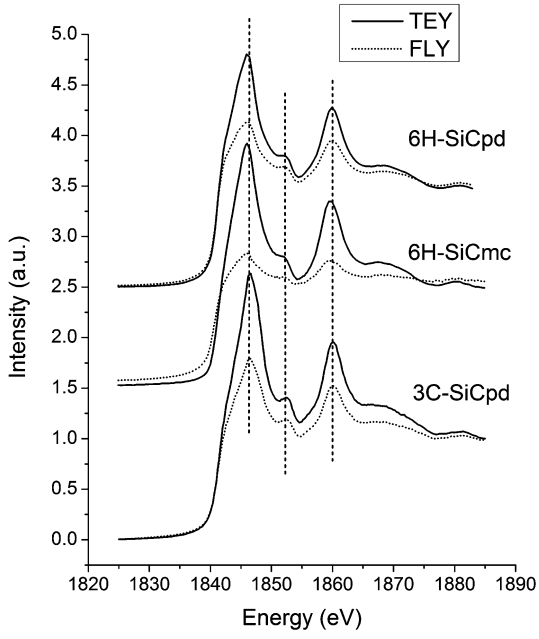

Figure 3. Si K-edge XANES of 6H-SiCpd, 6H-SiCmc, and 3C-SiCpd.

XANES of 3C-SiC displays similar features as its 6H-phase counterpart. This is not surprising as both SiC polytypes share the same Si−C tetrahedral local structures. A closer examination reveals that the resonances of the 3C-phase are slightly narrower than those of the 6H-phase, indicating that the interaction between the tetrahedral units in the 3C-SiC structure is less extensive than that in the 6H-SiC structure.

The calculated partial DOS of the Si site on both 6H-SiC and 3C-SiC is shown in Figure 4a. It can be seen that although SiC polytypes have same local Si−C structure, the DOS gets more complicated with increasing crystal packing complexity. The band gap can be clearly seen from the calculated DOS on both 6H-SiC and 3C-SiC, and four main bands in the unoccupied DOS (resonances in XANES) within the first 15 eV in the conduction band are in good agreement with the experimental results. The calculated Si K-edge XANES together with the experimental TEY are shown in Figure 4b. It can be seen that the experimental spectra are reasonably well reproduced by the DFT calculation, though the observed peaks are slightly broadened. A more noticeable pre-edge shoulder can be seen in 6H-SiC from calculated XANES than in 3C-SiC, this can explain the 1845 eV peak is broader in 6H-SiC than that in 3C-SiC.

The XANES spectra of the as-prepared core−shell nanowires, SiC/SiO_2-nw and SiCnw with the SiO_2 shell removed, are shown in Figure 5a. In SiC/SiO_2-nw, both TEY and FLY display a shoulder at 1841 eV, which is at the same location as that observed in 3C-SiCpd. However, the peak of maximum intensity is found at 1848 eV, instead of at 1845 eV, followed by two broad resonances at energies between 1855 and 1870 eV. The 1848 eV peak is attributed to the characteristic whiteline of SiO_2[46] from the outer shell of the SiC/SiO_2 core−shell nanowire. After HF treatment, this peak no longer exists and the XANES show all the characteristics of 3C-SiC, in good agreement with the XANES of SiC (Figure 3). Figure 5b shows a detailed comparison of SiC/SiO_2-nw and SiCnw. A difference curve was obtained by subtracting SiC contributions in the core−shell SiC after normalization of both spectra to the SiC edge jump. Thermally oxidized Si nanowires are used as the reference of SiO_2. It can be seen that the 1848 eV whiteline and shape resonance around 1865 eV in the difference curve are identical to the SiO_2 features. The edge jump of the normalized TEY spectra of SiC/SiO_2-nw and SiCnw has a ratio of about 3:1, which means that the oxide layer is relatively thick (SiO_2:SiC $\sim$ 2:1) in agreement with the TEM results (Figure 1). Thus the SiO_2 shell has a significant contribution to the SiC/SiO_2-nw TEY. However, as shown below, the oxide shell can be removed successfully by HF treatment.

C K-edge XANES. The C K-edge XANES of 6H-SiCpd, 6H-SiCmc and 3C-SiCpd are shown in Figure 6. It can be seen that all spectra have rich features at energy between 285 and 300 eV, which are assigned to the dipole transitions of C 1s to σ^* from sp^3 bonded carbon.[40] The TEY shows a pre-edge peak at 286.4 eV in 6H-SiCpd and 6H-SiCmc. The peak at this region is usually assigned to 1s to π^* transition. As TEY is surface sensitive, the peak may be due to the presence of defect at surface, in which C is sp^2-bonded.[47,48] The TEY of 3C-SiCpd shows some spikes at pre-edge, this is due to charging at the surface, as it is not observed in FLY.[49] It can be seen in the calculated DOS, shown in Figure 7a that the valence charge distribution in SiC is strongly accumulated around the carbon atoms, in comparison with the Si DOS (Figure 5a), in agreement with previous calculations.[7] Also, as the photon flux and the absorption coefficient at Si K-edge are significantly lower than C K-edge,[28,50] no charging effect is observed at Si K-edge XANES.

The FLY of all three samples display similar features with maximum absorption around 290 eV, marked by dash line in Figure 6, but the peaks are slightly narrowed in 3C-SiCpd. In FLY, the pre-edge shoulder is apparent at 285.4 eV in 3C-SiCpd, but it shifts to 286.2 eV in 6H-SiC, marked as dotted line. This $\sim$0.8 eV difference can be attributed to the difference in band gap energy between 6H- and 3C-SiC. The same discrepancy

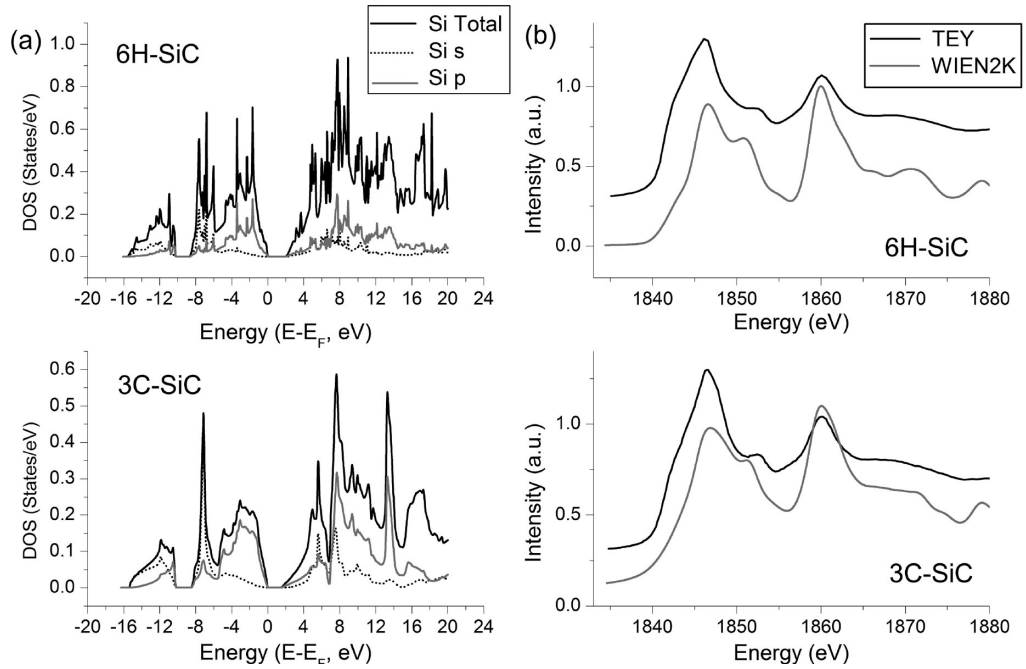

Figure 4. (a) Calculated Si DOS of 6H-SiC (upper panel) and 3C-SiC (lower panel); (b) comparison of Si K-edge XANES using WIEN2k and experimental TEY of 6H-SiC (upper panel) and 3C-SiC (lower panel).

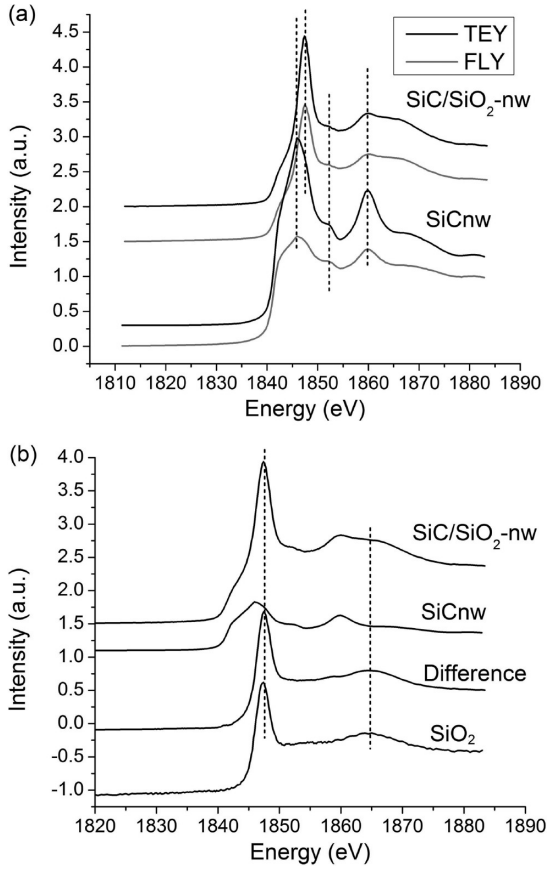

Figure 5. (a) Si K-edge XANES of SiC/SiO_2-nw and SiCnw; (b) comparison of SiC/SiO_2-nw, SiCnw, difference curve between SiC/SiO_2-nw and SiCnw with thermally oxidized Si.

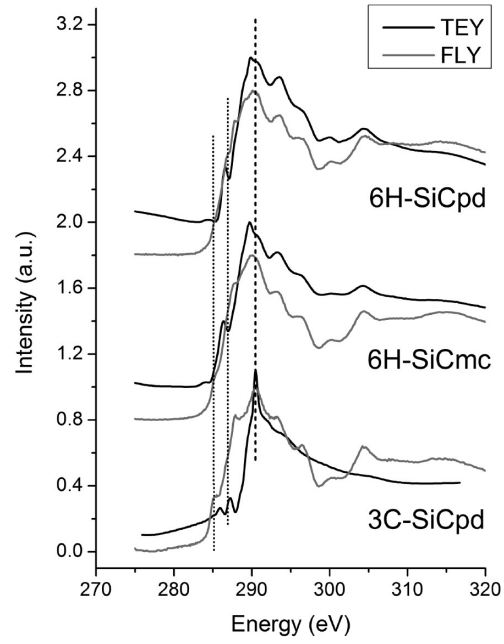

Figure 6. C *K*-edge XANES of 6H-SiCpd, 6H-SiCmc, and 3C-SiCpd.

can also be clearly identified from the DOS calculation (Figure 7a), in which 3C-SiC reveals a narrower band gap than that in 6H-SiC. Additionally, as the strongest contribution to the total DOS in the conduction band comes from Si s and C p bands,[8] seen from Figures 5a and 7a, this explains why the edge jump differences can be more readily observed at the C K-edge but not obvious enough to be seen in Si K-edge (1s to p transition).

Figure 7b shows the comparison of the experimental FLY with theoretical calculations. It can be seen that the calculated spectra reproduce the features reasonably well in the near-edge region, i.e., below 300 eV. The resonances around 290 eV are sharper in 3C-SiC than in 6H-SiC, but the relative intensities of the peaks are not quite the same as the experimental results. Also, unlike the experimental FLY, the pre-edge features are clearly present in both 3C- and 6H-SiC. These discrepancies can be partly due to vibrational broadening and partly due to energy dependent final state lifetime.[51]

The C K-edge XANES of the as-prepared (core−shell) and the HF-treated SiC nanowire (SiCnw) samples are shown in

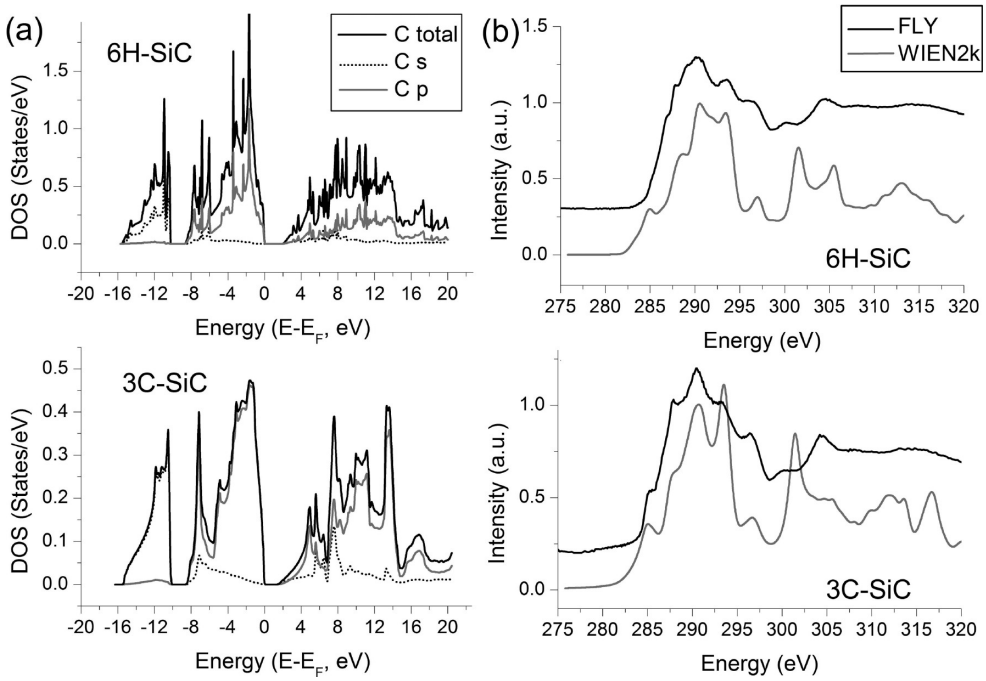

Figure 7. (a) C DOS calculation of 6H-SiC (top panel) and 3C-SiC (bottom panel); (b) C *K*-edge DFT calculation and experimental C K-edge FLY of 6H-SiC (top panel) and 3C-SiC (bottom panel).

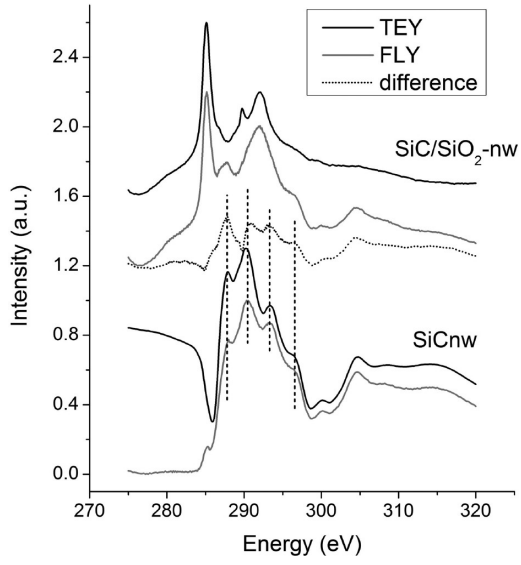

Figure 8. C K-edge XANES of SiC/SiO_2-nw and SiCnw.

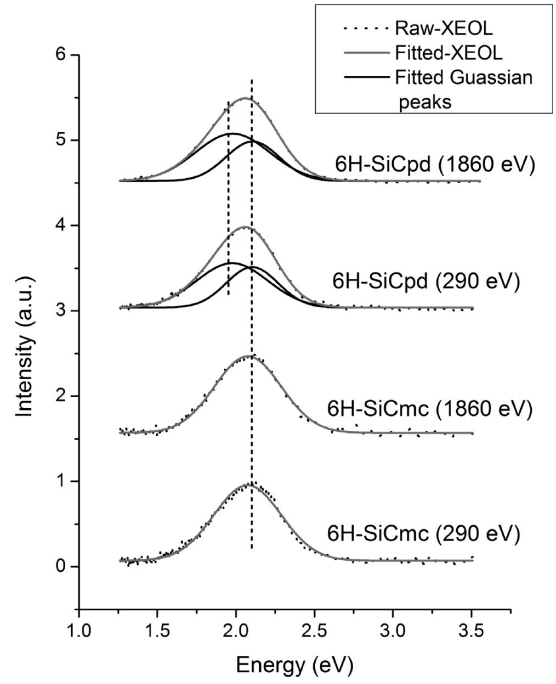

Figure 9. Normalized XEOL of 6H-SiCpd and 6H-SiCmc with excitation photon energy above Si K-edge and C K-edge, respectively.

Figure 8. At first glance the XANES look quite different before and after HF-treatment. In SiCnw, the spectra display all the resonances which have been observed in 3C-SiCpd (Figure 6), although charging problem exists in TEY, shown as a dip when the excitation energy is approaching the edge. However, SiC/SiO_2-nw has a sharp peak at 286 eV and another peak at 292 eV in both TEY and FLY, neither of which is present after HF-treatment. These peaks are almost certainly due to impurities containing sp^2 bonded C from the ambient. Assuming the impurities were on the surface of the nanowires, a difference curve is obtained by subtracting TEY from FLY after normalization to the π^* peak. This procedure allows minimizing the surface carbon contamination assuming that the FLY contains signal from both surface and bulk whereas TEY contains mostly surface signal. From Figure 8 we see that the difference curve clearly reveals all major features of SiC. This observation further confirms that the impurities were mainly present on the surface and the removal of SiO_2 shell using HF also removed the surface impurities. The SiCnw XANES features are clearly characteristic of the 3C-SiC phase, in agreement with the XRD results and previous observation. This observation confirms that while 6H-SiC is more stable in the bulk, the 3C-SiC phase can be more stable in nanostructures.[17−21]

2. Optical Properties. ***XEOL of 6H-SiC.*** The XEOL spectra of 6H-SiCpd and 6H-SiCmc are shown in Figure 9, with the excitation energy at 1860 and 290 eV, which are above the Si K-edge and C K-edge, respectively. The spectra are background subtracted and normalized to the incident photon flux. Upon

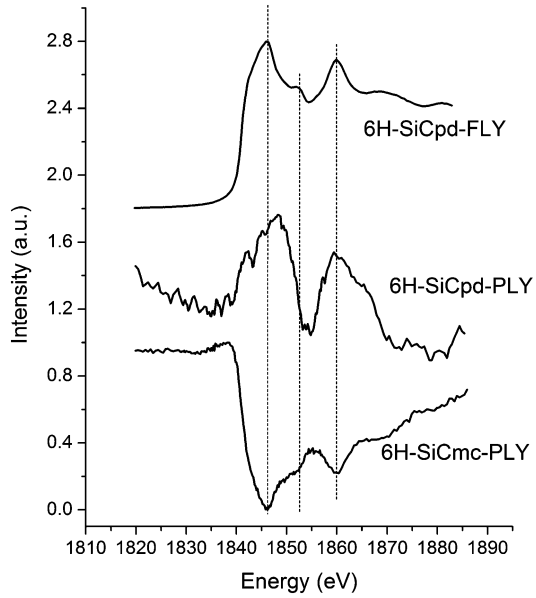

Figure 10. Si K-edge PLY of 6H-SiCpd (~1 μm crystallite) and 6H-SiCmc (~50 μm crystal), Si K-edge FLY of 6H-SiCpd is also shown for comparison.

excitation, both 6H-SiCpd and 6H-SiCmc emit bright luminescence, shown as a broad peak at energy around 2.0 eV (620 nm), which is lower than the band gap energy of 6H-SiC (3.02 eV). At first glance, the luminescence has no apparent difference between these two samples. However, if we look at the peak profile in details, we see that the XEOL for 6H-SiCpd, excited at both Si and C K-edge, can be fitted using two Gaussian peaks with comparable intensities, located at 1.98 eV (626.3 nm) and 2.09 eV (593.3 nm), while there is only one contribution at 2.08 eV in 6H-SiCmc. Since PL at wavelength slightly longer than 600 nm has been observed from bulk 6H-SiC,[14,15] the 2.09 eV emission in our case can be assigned to defect from the bulk. Note that this emission is independent of crystal sizes beyond nanoscale. Considering the average size of 6H-SiCmc is on the order of a micrometer, it is more "bulk-like" than 6H-SiCpd, thus only one emission peak is observed. However, unlike the relatively weak intensity in PL, both 6H-SiC samples in our case exhibit intense luminescence upon excitation at Si K- and C K-edges. The enhancement of luminescence could be either due to the large flux of the incident X-ray, or due to decreased crystal sizes, which lead to more localized defect sites.

The 1.98 eV emission observed from 6H-SiCpd, can be attributed to surface state, as the 6H-SiCpd has a large surface-to-volume ratio due to a decreased crystal size. This notion will be further advanced by the PLY XANES discussed below. XEOL with excitation energy below the edges yield similar profiles albeit with different intensities (not shown). Since at the C K-edge, the XANES can be interfered by the existence of carbon impurities, the following analysis is focused on the Si K-edge.

In Figure 10, the PLY of 6H-SiCpd and 6H-SiCmc were collected as total luminescence (zero order) with the excitation energy scanned stepwise across the Si K-edge, and the FLY of 6H-SiCpd was included as the reference. The edge jump of the PLY XANES of 6H-SiCpd appears at 1842 eV, followed by two main resonances centered at 1848.2 and 1860 eV. Compared to the FLY of 6H-SiCpd, the first peak exhibits similar profile in PLY but is broadened. The peak maximum is 2.2 eV blue-shifted, where the energy position is normally observed for the whiteline of SiO_2. The second peak is at the same position as FLY, but a shoulder can also be seen at energy around 1864 eV. Although the SiO_2 features are not apparent in the XANES of 6H-SiCpd (Figure 3), its presence on the surface can be revealed in the PLY XANES if the optical decay in the SiO_2 channel is intense and efficient. Note that the small peak at 1852 eV is hardly observed in PLY. The possible reason for that is partly due to its weak intensity and the interference of the strong SiO_2 whiteline and partly due to saturation effect. While the coexistence of SiC and surface SiO_2 could explain the blue-shift of the first peak maxima and the broad shoulder at higher energy and in agreement with the observation of two contributions in XEOL, where the 2.09 eV is from SiC and the 1.98 eV arises from SiC-SiO_2 interface, the saturation effect also contributes as we can see from Figure 3 where the saturation effect in the FLY is most severe in 6H-SiCmc, less so in 6H SiCpd but not negligible.

The PLY of 6H-SiCmc displays all characteristics of SiC, though inverted. Recall that there is only one contribution in XEOL (Figure 9). Thus the PLY XANES tracks the intensity evolution of the 2.08 eV emission from SiC. The inversion of the PLY XANES is caused by saturation effect resulting from total absorption,[52] which happens in the case of relatively thick samples, as the size of 6H-SiCmc (~50 μm) is relatively larger compared to that of 6H-SiCpd (~1 μm). This observation is consistent with the results shown in Figure 3.

XEOL of 3C-SiC. The XEOL of three 3C-SiC samples with excitation energy at 1860 and 290 eV are shown in Figure 11. It can be seen that for each 3C-SiC, the luminescence from both Si K-edge and C K-edge are quite similar with only a slight difference in the branching ratio. Unlike the bright luminescence from 6H-SiC, 3C-SiCpd only emits weakly upon excitation. The luminescence has a broad peak which can be fitted into two Gaussian peaks centered at 2.07 eV (599 nm) and 2.75 eV (451 nm). The 2.07 eV emission is very similar to the one observed from 6H-SiC (Figure 9) and can be assigned to the defect from the bulk, and this peak is independent of crystal phases and excitation energy. The 2.75 eV emission is only observed in the 3C-phase, and the intensity varies at both the Si and at C K-edge. Thus this 2.75 eV emission is more likely from the surface. The luminescence from both SiC/SiO_2-nw and SiCnw exhibit similar spectra: an asymmetric peak with highest intensity at 2.65 eV (468 nm). The Ga;ussian fit shows that for SiC/SiO_2-nw, the luminescence is composed of a broad peak at 2.44 eV (508 nm), a relatively sharp peak at 2.70 eV (459 nm), and a very weak peak at 3.30 eV (375 nm). The intensity of the 3.30 eV peak increases slightly when excited above C K-edge. The first two peaks are also found at the same location for SiCnw, but the intensity of the 2.70 eV peak drops. The 3.30 eV peak disappears in SiCnw.

Since luminescence from 3C-SiC covers a broad range of wavelengths and the shoulder is distinguishable from the main peak, it is desirable to track the XANES with partial luminescence yield as well as total luminescence (zero order) to enhance the site specificity. Since the weak luminescence results in a low signal-to-noise ratio, thus instead of measuring the PLY XANES with an optical window while scanning the excitation energy continuously, the PLY XNES was obtained, one point at a time, according to the fitted peak areas in the XEOL spectra recorded at selected excitation energies across the Si *K*-edge.

Let us first look at each of the PLY XANES of 3C-SiCpd shown in Figure 12 where the PLY XANES, from bottom to top, were collected at zero order (300−800 nm), the 2.75 eV emission and the 2.07 eV emission respectively; the TEY is shown as reference. Although the intensity is weak, the zero

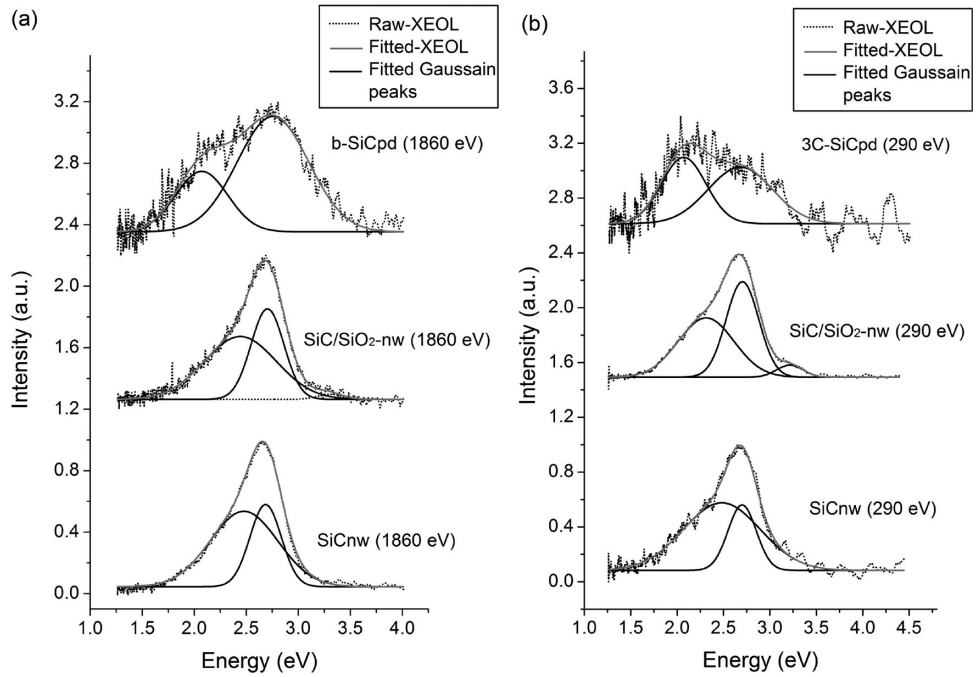

Figure 11. Normalized XEOL of 3C-SiCpd, SiC/SiO_2-nw, and SiCnw with Gaussian fittings with excitation photon energy (a) above Si K-edge; (b) above C K-edge.

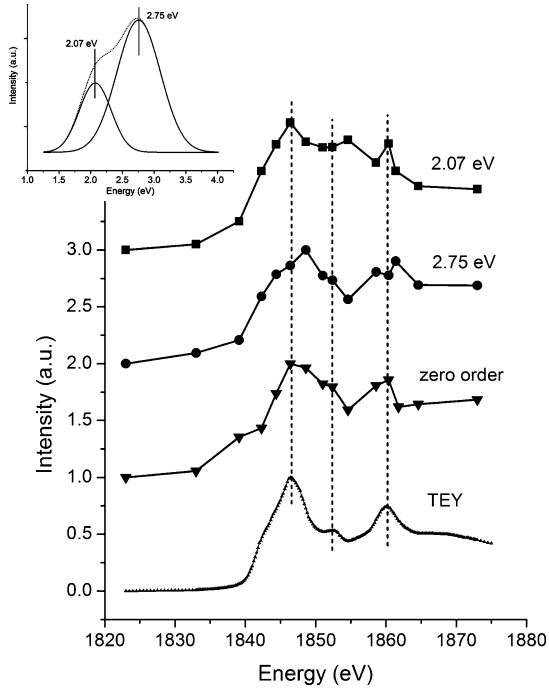

Figure 12. Region selected PLY of 3C-SiCpd, in which the intensity of fitted emission peaks (by peak areas) is plotted against the excitation energy, and TEY of 3C-SiCpd is shown as reference. XEOL with fitted peaks is shown in inset.

order luminescence shows similar characteristic resonance as TEY, marked with dashed lines. The 2.07 eV luminescence shows the edge jump at 1842 eV, and a peak maximum at 1846 eV, followed by weak oscillations above the edge. The 2.75 eV luminescence, which has higher contribution in the XEOL spectra, exhibit a shoulder at 1845 eV followed by peak maximum at 1848 eV. Thus this 2.75 eV emission can be attributed to the localized defect on the surface in which both SiC and SiO_2 contribute to the light emission. In fact, the emission at 2.75 eV has also been observed from 3C-SiC particles in $Si_{1-x}C_x$:H matrix,[53] and attributed to the optical emission from defect states on the surface. The 3C-SiC has larger surface area, which can explain increase sensitivity of an oxidized surface and its contribution to PLY-XANES.

Figure 13 shows the PLY XANES of the core−shell 3C-SiC/SiO_2 nanowires and the HF-treated SiCnw. Luminescence at the three subregions were plotted for SiC/$SiCO_2$-nw, shown in Figure 13a, compared with TEY of SiC/SiO_2-nw and 3C-SiCpd. It can be seen from zero order PLY that SiC/SiO_2-nw shows an increase in luminescence intensity as the excitation energy approaches the edge, followed by small variations above the edge and a broad peak at higher energy (i.e., around 1860 eV). Since SiC and SiO_2 are both present in the core−shell nanowires, there is a competition for the incoming photon when the excitation energy scans across the Si edge, thus TEY and FLY show a combined feature of the two components. The 2.44 eV luminescence partial PLY, however, exhibits all features of SiC, while the 2.70 eV luminescence does not show a significant edge jump until the excitation energy reaches the SiO_2 whiteline at 1848 eV. As has been observed in Si nanowires[26] and SiO_2 nanowires,[54] the 2.70 eV emission is known to originate from SiO_2 oxygen vacancy. This is in agreement with our PLY spectra. The 2.44 eV emission can be attributed to SiC nanowires core due to quantum confinement.

Let us now investigate how these luminescence peaks can be associated with the electronic structure of the SiC/SiO_2-nw core−shell nanostructure. Using the effective mass approximation, the band gap of semiconductor clusters E_g^* can be described as a function of particle radius as follows:[55]

$$E_g^* = E_g + \frac{\hbar^2\pi^2}{2R^2}\left[\frac{1}{m_e} + \frac{1}{m_h}\right] - \frac{1.8e^2}{4\pi\varepsilon_0\varepsilon R}$$

In the case of 3C-SiC, E_g is the band gap of bulk 3C-SiC (2.39 eV), R is the diameter of the nanowires (5 nm), ε is the dielectric constant of 3C-SiC (9.72),[56] m_e and m_h are the mass of the electron and hole, respectively, which makes the reduced

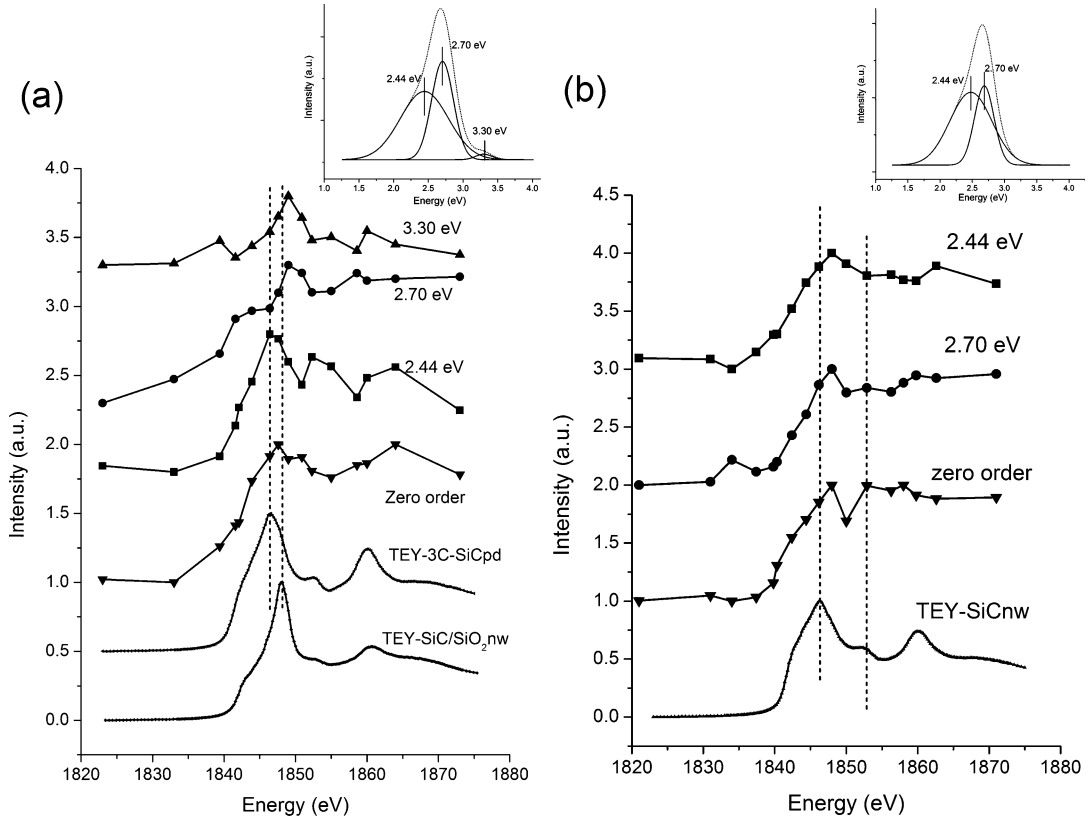

Figure 13. Region selected PLY of (a) SiC/SiO_2-nw, (b) SiCnw. The insets show the XEOL spectra with fitted peaks.

mass of the electron−hole pair (exciton). For 3C-SiC, $m_e = 0.394m_0$ and $m_h = 0.387m_0$ is used while m_0 is the mass of free electron.[57] The band gap thus calculated for SiCnw is 2.41 eV, which is very close to the observed 2.44 eV.

The 3.30 eV emission, though the intensity is fairly weak compared to the total light emission, reaches its highest intensity after the SiO_2 channel turns on. Luminescence at shorter wavelength has been observed from the photoluminescence spectrum of magnetron sputtered SiO_2 films annealed at high temperature.[58] We attribute the origin of the emission to defect center in SiO_2,[59] as this peak disappears after HF treatment (Figure 11).

The PLY of SiCnw is shown in Figure 13b. All three PLY (zero oder, 2.44 eV, and 2.70 eV emission) yield similar spectra. They all show the characteristic, round rising edge of SiC although, the presence of the SiO2 whiteline is still noticeable. As shown in XEOL (figure 11b), the intensity of the 2.70 eV emission decreases considerably after HF treatment. The two peaks from the fit overlap significantly. It is interesting to note that there is no SiO_2 features observed from TEY of SiCnw, thus HF-treatment of the core−shell SiCnw removed most of SiO_2 shell. Howver, the optical signal suggests that some surface oxide remains, which contribute to the 2.70 eV luminescence. Meanwhile, the 2.44 eV luminescence from SiC is still present, but with weaker intensity.

Conclusion

We have reported the Si K-edge and C K-edge XANES and XEOL studies of SiC of hexagonal (6H) and cubic (3C) crystal of micro and nanostructures. This study reveals that for all SiC crystals, the near-edge structures have similar features at both Si and C K-edges, as SiC polytypes share the same Si−C local tetrahedral structure. We have observed that the 6H- and 3C-SiC polytypes exhibits a 0.8 eV difference in the C K threshold, and we attributed it to the difference in the band gap energy. In comparison with the theoretical calculations using DFT, the calculated Si K-edge XANES show excellent agreement with the experimental results, but for the C K-edge, only semiquantitative results are reproduced by theory. As for the core−shell SiC nanowires, both SiC and SiO_2 resonances can be seen at the Si K-edge, while upon the removal of SiO_2, the core SiC nanowires display the typical XANES features of 3C-SiC. Both XRD and XANES results confirm that 3C-SiC nanostructure is stable. It is also found that SiC materials emit light at different wavelengths ranging from 375 to 700 nm depending on the crystal structures and the morphologies. But for the same sample, luminescence exhibits similar profile upon excitation across both Si K- and C K-edge, though there are slight variations in the relative intensities of the emission peaks. The light emission at 2.07 eV can be observed from all SiC crystallines regardless of phases (i.e., 6H-SiCpd, 6H-SiCmc, and 3C-SiCpd). The origin of this emission is attributed to the SiC bulk defect. For 6H-SiCpd, additional defect luminescence from surface (1.98 eV) due to a reduced crystal size also contributes to the light emission. On the other hand, 3C-SiC nanocrystals exhibit weak luminescence which is composed of two emission bands: one is from bulk defect of SiC (2.07 eV), similar to what is observed in 6H-SiC, and the other (2.75 eV) is from surface states. Three contributions found in core−shell 3C-SiC nanowires arise almost certainly from SiO_2 in the shell (2.70 and 3.30 eV), core−shell interface and SiC of quantum confinement (2.44 eV). Once the core−shell nanowires were treated with HF, the 2.70 and 2.44 eV emissions were still observable, albeit with reduced intensity while the 3.30 eV emission was no longer present, as HF removed most of the surface SiO_2, only SiC core and SiC-SiO_2 interface contributed to the light emission.

Finally, we have shown that the combined use of XANES and XEOL techniques provides an unique capability to inves-

tigate nanostructure, especially light emitting nanomaterials. These capabilities should be applicable to the characterization of a wide variety of materials.

Acknowledgment. Research at the University of Western Ontario is supported by NSERC, CRC, CFI, and OIT. The Canadian Light Source is supported by CFI, NSERC, NRC, CHIR, and the University of Saskatchewan. Assistance from Tom Regier, the SGM beamline scientist is gratefully acknowledged. Research at Shanghai Jiao Tong University is supported by National Natural Science Foundation of China No. 50730008 and Shanghai Science and Technology Foundation No: 09JC1407400.

References and Notes

(1) Harris, C. I.; Savage, S.; Konstantinov, A.; Bakowski, M.; Ericsson, P. *Appl. Surf. Sci.* **2001**, *184*, 393.
(2) Nakamura, D.; Gunjishima, I.; Yamaguchi, S.; Ito, T.; Okamoto, A.; Kondo, H.; Onda, S.; Takatori, K. *Nature (London, U. K.)* **2004**, *430*, 1009.
(3) Ching, W. Y.; Xu, Y. N.; Rulis, P.; Ouyang, L. *Mater. Sci. Eng., A* **2006**, *422*, 147.
(4) Bhatnagar, M.; Baliga, B. J. *IEEE Trans. Electron. Devices* **1993**, *40*, 645.
(5) Zhou, W.; Yan, L.; Wang, Y.; Zhang, Y. *Appl. Phys. Lett.* **2006**, *89*, 013105/1.
(6) Park, C. H.; Cheong, B.-H.; Lee, K.-H.; Chang, K. J. *Phys. Rev. B* **1994**, *49*, 4485.
(7) Persson, C.; Lindefelt, U. *J. Appl. Phys.* **1997**, *82*, 5496.
(8) Bernstein, N; Gotsis, H. J.; Papaconstantopoulos, D. A.; Mehl, M. J. *Phys. Rev. B* **2005**, *71*, 075203/1.
(9) Kackell, P.; Wenzien, B.; Bechstedt, F. *Phys. Rev. B* **1994**, *50*, 10761.
(10) Fan, J. Y.; Wu, X. L.; Chu, P. K. *Prog. Mater. Sci.* **2006**, *51*, 983.
(11) Choyke, W. J.; Patrick, L. *Phys. Rev. B* **1970**, *2* (3), 4959.
(12) Ikeda, M.; Matsunami, H.; Tanaka, T. *Phys. Rev. B* **1980**, *22*, 2842.
(13) Matsumoto, T.; Takahashi, J.; Tamaki, T.; Futagi, T.; Mimura, H. *Appl. Phys. Lett.* **1994**, *64*, 226.
(14) Petrova-Koch, V.; Sreseli, O.; Polisski, G.; Kovalev, D.; Muschik, T.; Koch, F. *Thin Solid Films* **1995**, *255*, 107.
(15) Jessensky, O.; Mueller, F.; Goesele, U. *Thin Solid Films* **1997**, *297*, 224.
(16) Konstantinov, A. O.; Henry, A.; Harris, C. I.; Janzen, E. *Appl. Phys. Lett.* **1995**, *66*, 2250.
(17) Guo, Y. P.; Zheng, J. C.; Wee, A. T. S.; Huan, C. H. A.; Li, K.; Pan, J. S.; Feng, Z. C.; Chua, S. J. *Chem. Phys. Lett.* **2001**, *339*, 319.
(18) Zhao, J.; Mao, D. S.; Lin, Z. X.; Jiang, B. Y.; Yu, Y. H.; Liu, X. H.; Wang, H. Z.; Yang, G. Q. *Appl. Phys. Lett.* **1998**, *73*, 1838.
(19) Seong, H.-K.; Choi, H.-J.; Lee, S.-K.; Lee, J.-I.; Choi, D.-J. *Appl. Phys. Lett.* **2004**, *85*, 1256.
(20) Niu, J. J.; Wang, J. N. *J. Phys. Chem. B* **2007**, *111*, 4368.
(21) Rebohle, L.; Gebel, T.; Frob, H.; Reuther, H.; Skorupa, W. *Appl. Surf. Sci.* **2001**, *184*, 156.
(22) Chen, D.; Liao, Z. M.; Wang, L.; Wang, H. Z.; Zhao, F.; Cheung, W. Y.; Wong, S. P. *Opt. Mater. (Amsterdam, Neth.)* **2003**, *23*, 65.
(23) Tang, Y. H.; Sham, T. K.; Yang, D.; Xue, L. *Appl. Surf. Sci.* **2006**, *252*, 3386.
(24) Sham, T. K.; Jiang, D. T.; Coulthard, I.; Lorimer, J. W.; Feng, X. H.; Tan, K. H.; Frigo, S. P.; Rosenberg, R. A.; Houghton, D. C.; Bryskiewicz, B. *Nature* **1993**, *363*, 331.
(25) Liu, L.; Ko, J. Y. P.; Ward, M. J.; Yiu, Y. M.; Sham, T. K.; Zhang, Y. *J. Phys.: Conf. Ser.* **2009**, *190*,
(26) Sham, T. K.; Naftel, S. J.; Kim, P. S. G.; Sammynaiken, R.; Tang, Y. H.; Coulthard, I.; Moewes, A.; Freeland, J. W.; Hu, Y. F.; Lee, S. T. *Phys. Rev. B* **2004**, *70*, 045313.
(27) Weimin, Z.; Xuan, L.; Yafei, Z. *Appl. Phys. Lett.* **2006**, *89*, 223124.
(28) Regier, T.; Paulsen, J.; Wright, G.; Coulthard, I.; Tan, K.; Sham, T. K.; Blyth, R. I. R. *AIP Conf. Proc.* **2007**, *879*, 473.
(29) Hohenberg, P.; Kohn, W. *Phys. Rev.* **1964**, *136*, B864.
(30) Kohn, W.; Sham, L. J. *Phys. Rev.* **1965**, *140*, A1133.
(31) Perdew, J. P.; Wang, Y. *Phys. Rev. B* **1992**, *45*, 13244.
(32) Blaha, P.; Schwarz, K. *J. Phys. F: Met. Phys.* **1987**, *17*, 899.
(33) Blaha, P.; Schwarz, K.; Sorantin, P.; Trickey, S. B. *Comput. Phys. Commun.* **1990**, *59*, 399.
(34) Momma, K.; Izumi, F. *J. Appl. Crystallogr.* **2008**, *41*, 653.
(35) Wyckoff, R. N. G. *Crystal Structure*; John Wiley & Sons: New York, 1963; Vol. 1.
(36) Rohrer, G. S. *Structure and Bonding in Crystalline Materials*; Cambridge University Press: Cambridge, 2001.
(37) Blochl, P. E.; Jepsen, O.; Andersen, O. K. *Phys. Rev. B* **1994**, *49*, 16223.
(38) *Unoccupied Electronic States: Fundamentals for XANES, EELS, IPS and BIS*; Fuggle, J. C.; Inglesfield, J. E., Eds.; Springer-Verlag: New York, 1992; Vol. 69.
(39) Prado, R. J.; D'Addio, T. F.; Fantini, M. C. A.; Pereyra, I.; Flank, A. M. *J. Non-Cryst. Solids* **2003**, *330*, 196.
(40) Chang, Y. K.; Hsieh, H. H.; Pong, W. F.; Tsai, M. H.; Dann, T. E.; Chien, F. Z.; Tseng, P. K.; Chen, L. C.; Wei, S. L.; Chen, K. H.; Wu, J. J.; Chen, Y. F. *J. Appl. Phys.* **1999**, *86*, 5609.
(41) Baba, Y.; Sekiguchi, T.; I., S.; Nath, K. G. *Appl. Surf. Sci.* **2004**, *237*, 176.
(42) Jaklevic, J.; Kirby, J. A.; Klein, M. P.; Robertson, A. S.; Brown, G. S.; Eisenberger, P. *Solid State Commun.* **1977**, *23*, 679.
(43) Zschech, E.; Troeger, L.; Arvanitis, D.; Michaelis, H.; Grimm, U.; Baberschke, K. *Solid State Commun.* **1992**, *82*, 1.
(44) Eisebitt, S.; Boeske, T.; Rubensson, J. E.; Eberhardt, W. *Phys. Rev. B* **1993**, *47*, 14103.
(45) X-ray Calculator. http://henke.lbl.gov/optical_constants.
(46) Kim, P. S. G.; Tang, Y. H.; Sham, T. K.; Lee, S. T. *Can. J. Chem.* **2007**, *85*, 695.
(47) Gutierrez, A.; Lopez, M. F.; Garcia, I.; Vazquez, A. *J. Vac. Sci. Technol.* **1997**, *15*, 294.
(48) Nithianandam, J.; Rife, J. C.; Windischmann, H. *Appl. Phys. Lett.* **1992**, *60*, 135.
(49) Charging at very intense light source can be a problem for recording XANES of non-conducting materials in the TEY mode. This problem can be miniminzed by reducing the flux with filters and increasing the dead time between steps. In this case, our samples are thin enough so that FLY, which is less susceptible to charging, is used for the analysis.
(50) McMaster, W. H. *Compilation of X-ray cross sections*; UCRL, 1969.
(51) Mueller, J. E.; Jepsen, O.; Wilkins, J. W. *Solid State Commun.* **1982**, *42*, 365.
(52) Sham, T. K.; Coulthard, I. *J. Synchrotron Radiat.* **1999**, *6*, 215.
(53) Wu, X. L.; Siu, G. G.; Stokes, M. J.; Fan, D. L.; Gu, Y.; Bao, X. M. *Appl. Phys. Lett.* **2000**, *77*, 1292.
(54) Yu, D. P.; Hang, Q. L.; Ding, Y.; Zhang, H. Z.; Bai, Z. G.; Wang, J. J.; Zou, Y. H.; Qian, W.; Xiong, G. C.; Feng, S. Q. *Appl. Phys. Lett.* **1998**, *73*, 3076.
(55) Brus, L. *J. Phys. Chem.* **1986**, *90*, 2555.
(56) Choyke, W. J.; Patrick, L. *Phys. Rev. B* **1970**, *2*, 4959.
(57) Wu, X. L.; Fan, J. Y.; Qiu, T.; Yang, X.; Siu, G. G.; Chu, P. K. *Phys. Rev. Lett.* **2005**, *94*, 026102.
(58) Song, H. Z.; Bao, X. M.; Li, N. S.; Wu, X. L. *Appl. Phys. Lett.* **1998**, *72*, 356.
(59) Kim, K.; Suh, M. S.; Kim, T. S.; Youn, C. J.; Suh, E. K.; Shin, Y. J.; Lee, K. B.; Lee, H. J.; An, M. H.; Ryu, H. *Appl. Phys. Lett.* **1996**, *69*, 3908.

JP100277S